

## Methods

# Focal plane array infrared imaging: a new way to analyse leaf tissue

Philip Heraud<sup>1,2</sup>, Sally Caine<sup>2</sup>, Gordon Sanson<sup>2</sup>, Ros Gleadow<sup>2</sup>, Bayden R. Wood<sup>1,3</sup> and Don McNaughton<sup>1,3</sup>

<sup>1</sup>Centre for Biospectroscopy, <sup>2</sup>School of Biological Sciences, and <sup>3</sup>School of Chemistry, Monash University, Clayton, Victoria 3800, Australia

### Summary

Author for correspondence:

Philip Heraud

Tel: +61 3 9905 4597

Fax: +61 3 9905 4597

Email: phil.heraud@sci.monash.edu.au

Received: 7 June 2006

Accepted: 7 August 2006

- Here, a new approach to macromolecular imaging of leaf tissue using a multichannel focal plane array (FPA) infrared detector was compared with the proven method of infrared mapping with a synchrotron source, using transverse sections of leaves from a species of *Eucalyptus*.
- A new histological method was developed, ideally suited to infrared spectroscopic analysis of leaf tissue. Spatial resolution and the signal-to-noise ratio of the FPA imaging and synchrotron mapping methods were compared.
- An area of tissue 350  $\mu\text{m}^2$  required approx. 8 h to map using the synchrotron technique and approx. 2 min to image using the FPA. The two methods produced similar infrared images, which differentiated all tissue types in the leaves according to their macromolecular chemistry.
- The synchrotron and FPA methods produced similar results, with the synchrotron method having superior signal-to-noise ratio and potentially better spatial resolution, whereas the FPA method had the advantage in terms of data acquisition time, expense and ease of use. FPA imaging offers a convenient, laboratory-based approach to microscopic chemical imaging of leaves.

**Key words:** eucalyptus, focal plane array, infrared imaging, leaf composition, synchrotron.

*New Phytologist* (2006) doi: 10.1111/j.1469-8137.2006.01881.x

© The Authors (2006). Journal compilation © *New Phytologist* (2006)

### Introduction

Traditional histology using light or electron microscopy has been limited mainly to resolving morphological features in cells and tissues because the chemical composition of the structures being imaged can, at best, only be inferred from interactions between cellular chemistry and stains or other added reagents. Microspectroscopic Fourier transform infrared (FTIR) mapping, however, allows macromolecular composition to be mapped directly without the possible confounding influences of added histological compounds. Most previous studies employing this technique have used synchrotron sources of infrared light because it is much brighter than conventional sources, allowing good signal-to-noise ratio (S/N) at very

small apertures, hence enabling the best spatial resolution to be achieved. This approach has proved to be a powerful technique for understanding structure and composition in a range of plant tissues including roots, stems, leaves and reproductive structures (see Dokken & Davis, 2005 for a review).

A number of drawbacks with synchrotron-based FTIR microspectroscopic mapping have prevented its routine use in plant biology. The main barriers have been the expense and limited access to synchrotrons and the fact that measurements are very slow (hours). A new technique known as focal plane array (FPA) infrared imaging (Bhargava & Levin, 2005) has recently become available and this promises virtually all the advantages of the synchrotron-based measurements with few

of the drawbacks. These systems are laboratory-based and inexpensive compared with synchrotron-based measurement systems and, because they employ two dimensional detector arrays, can acquire data in a fraction of the time required for the point-by-point spectral acquisition using synchrotron-based mapping.

The use of FPA infrared imaging systems to investigate plant tissues is a recent development (Barron *et al.*, 2005; Mills *et al.*, 2005); however, there have been no studies to date comparing the results achieved with the existing synchrotron-based method. In addition, no studies have reported analysis of higher plant leaves using FPA imaging systems. Because synchrotron infrared microspectroscopic mapping has been proven to give reliable information about biochemical composition and location in plant tissues, we used this as the standard against which measurements using a FPA system were judged.

We used transverse sections of *Eucalyptus botryoides* leaves as a test subject because they contain a range of tissue types within close proximity, which could be expected to display different biochemical compositions, hence providing useful comparative maps and images. We compared the spectral data acquired using the two techniques and the images produced using FPA with synchrotron-derived maps of the same region of tissue.

## Materials and Methods

### Plant material

Leaves were collected from a mature *Eucalyptus botryoides* Smith tree located on the Monash University (Clayton) campus. The leaves were taken from a single branch in a sunlit position. Only healthy mature leaves were sampled, which were immediately fixed.

### Histological method

We first investigated the suitability of a variety of possible histological techniques for the preparation of the leaf sections suitable for synchrotron infrared microspectroscopic mapping and FPA imaging. Cryogenic sectioning was rejected because it was found that the thickness of intact sections achievable using this method was limited to *c.* 30  $\mu\text{m}$ . These sections were far too thick for infrared spectroscopy, rendering them opaque to many infrared frequencies, resulting in band saturation. Attempts to cut thinner cryogenically prepared sections resulted in tearing of the tissue. The use of resin embedding methods, commonly employed for light microscopy of plant tissues, was also rejected because the resin compounds had a number of intense bands that obscured bands of biological origin (data not shown). We used formalin fixation, alcohol dehydration and paraffin embedding to prepare the leaf tissue for sectioning as this method had been successfully employed in the preparation of human tissue samples for infrared

microspectroscopic mapping and imaging (Bambery *et al.*, 2004; Wood *et al.*, 2005). We found that 4- $\mu\text{m}$ -thick sections were ideal for infrared microspectroscopic measurements when the sections were deposited onto tin oxide-coated, silver-doped glass slides (Low *e* slides; Kevley Technologies, Chesterland, OH, USA). The Low *e* slides were used because they have the advantage over traditional infrared substrates of being transparent to visible light, enabling light microscopy to be performed on the same sections that were analysed using FTIR microscopy. They are also inexpensive and disposable, compared with crystalline substrates such as zinc selenide or calcium fluoride. It was found after testing a number of sections of different thicknesses (data not shown) that 4- $\mu\text{m}$  sections enabled spectra with good signal-to-noise characteristics to be acquired without saturation of the most intense spectral bands. We found that 4- $\mu\text{m}$  transverse sections of *E. botryoides* leaves could be routinely achieved without tearing of the tissue using the paraffin embedding method. Spectra acquired from the Low *e* slides in reflectance mode involve a double pass through the sample; therefore the total path length through the *E. botryoides* sections was 8  $\mu\text{m}$ .

Specifically, whole leaves were harvested and immediately placed in saline-buffered 10% formalin solution for 24 h, with the formalin solution changed twice during that period. The fixed leaves were then dehydrated in 100% ethanol for 24 h, with two changes of ethanol, and then placed in 5% nitrocellulose/methyl benzoate solution for 24 h. Tissues were vacuum-embedded in paraffin wax for 4 h and left for 3 days in molten paraffin to allow full infiltration of the biological tissue.

The first set of sections were cut as follows. Before microtoming, the end of each wax block was soaked in Molliflex (a BDH tissue softening reagent; VWR International Limited, Poole, UK) for 20 min, and then cooled on ice for 20 min. Sections were cut at 4  $\mu\text{m}$  thickness and placed in a warm water bath to allow expansion of the paraffin wax and then transferred onto Low *e* slides. Nitrocellulose was removed from sections by placing the Low *e* slides in methyl benzoate for 20 min, followed by 4 h in xylene to remove paraffin, before infrared analysis.

The second set of sections were cut in a similar manner to the first, except without the use of nitrocellulose or Molliflex, and compared with the first set. The comparisons revealed no spectral evidence of nitrocellulose or Molliflex in the resulting sections (data not shown). We decided to use nitrocellulose and Molliflex because the addition of these components in the histological preparation resulted in sections that exhibited better tissue integrity, with minimal tearing during the cutting process.

### Synchrotron infrared microspectroscopy

FTIR absorption spectra were acquired using a Nicolet Thermo Electron Corporation, Waltham, MA, USA) Nic-Plan microscope with SpectraTech (Thermo Electron Corporation) 15 $\times$  Reflchromat Cassegrain objective attached

to a Nicolet (Thermo Electron Corporation) Magna 760 FTIR spectrometer, which was connected to infrared beamline 1.4.3 at the Advanced Light Source (ALS) synchrotron (Lawrence Berkeley National Laboratory, Berkeley, CA, USA). The infrared microscope employed a liquid nitrogen cooled mercury cadmium telluride detector (Nicolet MCT-A\*, Thermo Electron Corporation). The system was controlled using OMNIC 7.1 software (Thermo Electron Corporation) running on an IBM-compatible PC. The FTIR microscope was operated without an aperture; the region of the sample from which the spectral information was acquired was determined by the dimensions of the incoming collimated infrared beam from the synchrotron, which has been previously determined to be approximately circular with a diameter varying with wavelength (Martin & McKinney, 1998; Levenson *et al.*, 2006). An area of approx.  $350 \mu\text{m}^2$ , corresponding to the same region of tissue imaged using the focal plane array FTIR microscope, was mapped with a step interval of  $8 \mu\text{m}$ . Each spectrum was acquired in reflectance mode at spectral resolution of  $8 \text{ cm}^{-1}$  with 64 scans coadded. Apodization was performed using a triangular function. Each spectrum was referenced to a background spectrum acquired from a blank region of the substrate every 10 min. The measurement time for mapping the  $350 \mu\text{m}^2$  region was approx. 8 h.

### Focal plane array FTIR spectroscopic imaging

Spectral data were collected on a FTIR spectrometer (Model FTS 7000; Varian Inc., Palo Alto, CA, USA) coupled to an infrared microscope (model 600 UMA; Varian) using a  $15\times$  Varian objective and fitted with a liquid  $\text{N}_2$  cooled MCT  $64 \times 64$  element array Stingray (Varian) focal plane array detector. The Varian system was controlled by an IBM-compatible PC running WIN IR PRO 3.0 software (Varian). The absorbance spectra were acquired in reflectance mode at a spectral resolution of  $8 \text{ cm}^{-1}$  with 64 scans coadded. Apodization was performed using a triangular function. The system enabled 4096 spectra to be acquired from a sample area of approx.  $350 \mu\text{m}^2$  in approx. 2 min.

### Data processing and image analysis

Spectral array data were processed and images constructed using CYTOSPEC (Cytospec Inc., New York, NY, USA) version 1.2 infrared imaging software. Maps and images were contrasted showing either protein or lipid/lignin concentration. Protein concentration was determined from the integrated area of the amide I band, from  $1700$  to  $1580 \text{ cm}^{-1}$ , in baseline-corrected, vector-normalized spectra. Lipid concentration was determined from the integrated area of the ester carbonyl region, from  $1770$  to  $1700 \text{ cm}^{-1}$ , in baseline-corrected, vector-normalized spectra. Images and maps were contrasted using the 'Jet' colour scheme available in CYTOSPEC, with red indicating the strongest absorbance and blue the lowest.

### Measurements of spatial resolution and signal-to-noise ratio

Spatial resolution of the FPA system was determined at a wavelength of  $5 \mu\text{m}$  ( $2000 \text{ cm}^{-1}$ ) with a US Air Force target using the procedure outlined in Levenson *et al.* (2006) employing Rayleigh's criterion. The signal-to-noise ratios of 30 spectra extracted from the mesophyll tissue region in synchrotron maps and FPA images from the *E. botryoides* section were averaged. Signal-to-noise ratio was defined as the ratio of absorbance from the amide I band to the root mean square (RMS) of the noise from the region from  $2100$  to  $1900 \text{ cm}^{-1}$  in baseline-corrected spectra.

### Multivariate data analysis

Principal component analysis (PCA) was performed using UNSCRAMBLER 9.2 software (Camo, Oslo, Norway). Spectra were preprocessed using extended multiplicative signal correction (EMSC; Thenadill *et al.*, 2006) which normalizes spectra, accounting for differences in sample thickness, as well as removing baseline changes in the spectra resulting from light-scattering effects. PCA employed full cross validation. Scores plots were used to visualize any clustering of the samples, and loadings plots were used to determine which spectral region most contributed to the variance in the dataset.

## Results and Discussion

### Comparison of the FPA and synchrotron methods based on acquisition time and spectral quality

The comparison between the two methods was based on measurements using the same number of spectral scans (64), in which case the synchrotron technique required *c.* 8 h to map the same region imaged by the FPA in *c.* 2 min. Although the number of spectral scans used in the two methods was the same, not all the measurement time in each case was occupied by spectral acquisition. Approximately 75% of the total measurement time required for the synchrotron mapping was spectral acquisition and the remainder was stage movement. About 8% of the total measurement time for FPA imaging is occupied with spectral acquisition (M. Kansiz, pers. comm.). The best spatial resolution of synchrotron mapping achieved at the ALS beamline 1.4.3 facility has been reported to be approximately equal to half the measurement wavelength, and hence at  $2000 \text{ cm}^{-1}$  will be *c.*  $2.5 \mu\text{m}$  (Levenson *et al.*, 2006). Accordingly, the spatial resolution of the synchrotron maps of the *E. botryoides* leaf sections at  $2000 \text{ cm}^{-1}$  will be limited to the step length of  $8 \mu\text{m}$ . This implies that the spatial resolution of the synchrotron mapping of the leaf sections will be equivalent to the measured spatial resolution of the FPA imaging, which could just resolve  $7.8 \mu\text{m}$  on the test target at  $2000 \text{ cm}^{-1}$ .

The measured spatial resolution of the FPA imaging at  $2000\text{ cm}^{-1}$  is slightly inferior to the theoretical maximum spatial resolution which can be calculated by the Rayleigh criterion:

$$\text{Spatial resolution} = 1.22\lambda/2NA$$

( $\lambda$ , the measurement wavelength; NA, the numerical aperture of the objective optic.) The NA of the Varian 15 $\times$  objective was 0.5, giving a theoretical maximum resolution of 6.1  $\mu\text{m}$  at a wavelength of 5  $\mu\text{m}$ . Of course, both the measured and the theoretical maximum spatial resolutions at  $2000\text{ cm}^{-1}$  are greater than the projection area of each array detector onto the sample area, which is approx.  $5.5\text{ }\mu\text{m}^2$ . In practice, the spatial resolution of both techniques was good enough to resolve single cells in the leaf tissue.

Although the S/N of spectra acquired using the synchrotron was *c.* 12.5 times higher than that of FPA-derived spectra (635 vs 50), in practice, the spectral quality from the FPA system was still high enough to produce images of the leaf sections comparable to synchrotron maps, even when data were acquired over 2 min. Assuming that the S/N is directly proportional to the square root of averaged scans, the S/N of the FPA measurement would be equivalent to that of the synchrotron if the FPA measurement occurred for just over 5 h. This relationship does not hold in reverse, because a large proportion of the time required to acquire synchrotron maps involves translational movements of the sample stage rather than spectral acquisition. In practice, the spectral quality from

the FPA system was still high enough to produce images of the leaf sections comparable to synchrotron maps, even when data were acquired over 2 min (Figs 1, 2).

### Band assignments

The absorbance bands observed in the FTIR spectra from the *E. botryoides* leaf sections were similar to those observed in the FTIR spectra from leaves and other tissues of higher plant origin (Dokken & Davis, 2005). Figure 3 shows the average of the spectra from 40 points (locations) in the regions containing epidermal, mesophyll or conductive tissue from the FPA image of *E. botryoides*. The average spectra from the different tissue types from the leaves of another *Eucalyptus* species (*Eucalyptus viminalis* Labill.) were very similar (data not shown). Table 1 gives the assignment of the major bands that can be identified in the spectra shown in Fig. 3. Many of the bands observed are common to all biological tissues, arising from major macromolecular classes such as proteins, lipids and carbohydrates. For example, the amide bands attributable to proteins ( $1700\text{--}1500\text{ cm}^{-1}$ ), the C-O stretch bands mainly from carbohydrates ( $1200\text{--}900\text{ cm}^{-1}$ ) and the ester carbonyl from lipids (*c.*  $1730\text{ cm}^{-1}$ ), observed in spectra from all tissue regions of the leaf, also occur in the FTIR spectra of algal (Giordano *et al.*, 2001), bacterial (Kansiz *et al.*, 1999) and animal cells (Bambery *et al.*, 2004). However, some bands are unique to higher plant leaf tissue and were observed in spectra of the *E. botryoides* leaf, such as the bands attributable to lignin

**Table 1** The major bands present in the spectrum of *Eucalyptus botryoides* mesophyll cells from  $1800\text{ to }950\text{ cm}^{-1}$  (see Fig. 3)

Number in Fig. 3	Wavenumber ( $\text{cm}^{-1}$ )	Band assignment	Notes
1	<i>c.</i> 1730	$\nu(\text{C}=\text{O})$ (Nelson, 1991)	Primarily from ester functional groups from fatty acids, esters; and from lignin
2	<i>c.</i> 1650	Mainly $\nu(\text{C}=\text{O})$ from proteins (Nelson, 1991; Williams & Fleming, 1996)	Referred to as the amide I band
3	1620–1590	$\nu_{\text{as}}(\text{COO}^-)$ mainly from pectins (Bociek & Welti, 1975; Kačuráková & Wilson, 2001) $\nu(\text{C}=\text{C})$ from lignins (Faix, 1992; Himmelsbach <i>et al.</i> , 1998)	$\nu(\text{C}=\text{C})$ aromatic skeletal vibration referred to as the quadrant ring stretch (Colthup <i>et al.</i> , 1964)
4	<i>c.</i> 1545	Mainly $\nu(\text{C}-\text{H})$ and $\delta(\text{N}-\text{H})$ from proteins (Nelson, 1991; Williams & Fleming, 1996)	Referred to as the amide II band
5	<i>c.</i> 1515	$\nu(\text{C}=\text{C})$ , from lignins (Faix, 1992; Himmelsbach <i>et al.</i> , 1998)	Aromatic skeletal vibration referred to as the semicircle ring stretch (Colthup <i>et al.</i> , 1964)
6	<i>c.</i> 1450	$\delta_{\text{as}}(\text{CH}_3)$ and $\delta_{\text{as}}(\text{CH}_2)$ from proteins lipids, lignin (Zeroual <i>et al.</i> , 1994; Faix, 1992)	
7	<i>c.</i> 1420	$\nu_{\text{s}}(\text{COO}^-)$ mainly from pectins (Kačuráková & Wilson, 2001)	
8	<i>c.</i> 1370	$\delta_{\text{s}}(\text{CH}_3)$ and $\delta_{\text{s}}(\text{CH}_2)$ from proteins, lipids and lignin (Nelson, 1991; Zeroual <i>et al.</i> , 1994)	
9	<i>c.</i> 1320	Mainly $\nu(\text{C}-\text{H})$ and $\delta(\text{N}-\text{H})$ from proteins (Bandekar, 1992)	Referred to as the amide III band
10	<i>c.</i> 1270	Mainly $\nu(\text{C}-\text{C})$ , $\nu(\text{C}-\text{O})$ from carbohydrates and lignins (Faix, 1992)	
11	<i>c.</i> 1225	$\nu(\text{C}-\text{C})$ , $\nu(\text{C}-\text{O})$ , $\nu(\text{C}-\text{O})$ from lignins (Faix, 1992)	
12–15	1200–1000	Mainly $\nu(\text{C}-\text{O}-\text{C})$ of polysaccharides (Cael <i>et al.</i> , 1975; Wong <i>et al.</i> , 1991; Zeroual <i>et al.</i> , 1994; Kačuráková <i>et al.</i> , 2000)	

$\nu_{\text{as}}$ , asymmetric stretch;  $\nu_{\text{s}}$ , symmetric stretch;  $\delta_{\text{as}}$ , asymmetric deformation (bend);  $\delta_{\text{s}}$ , symmetric deformation (bend).

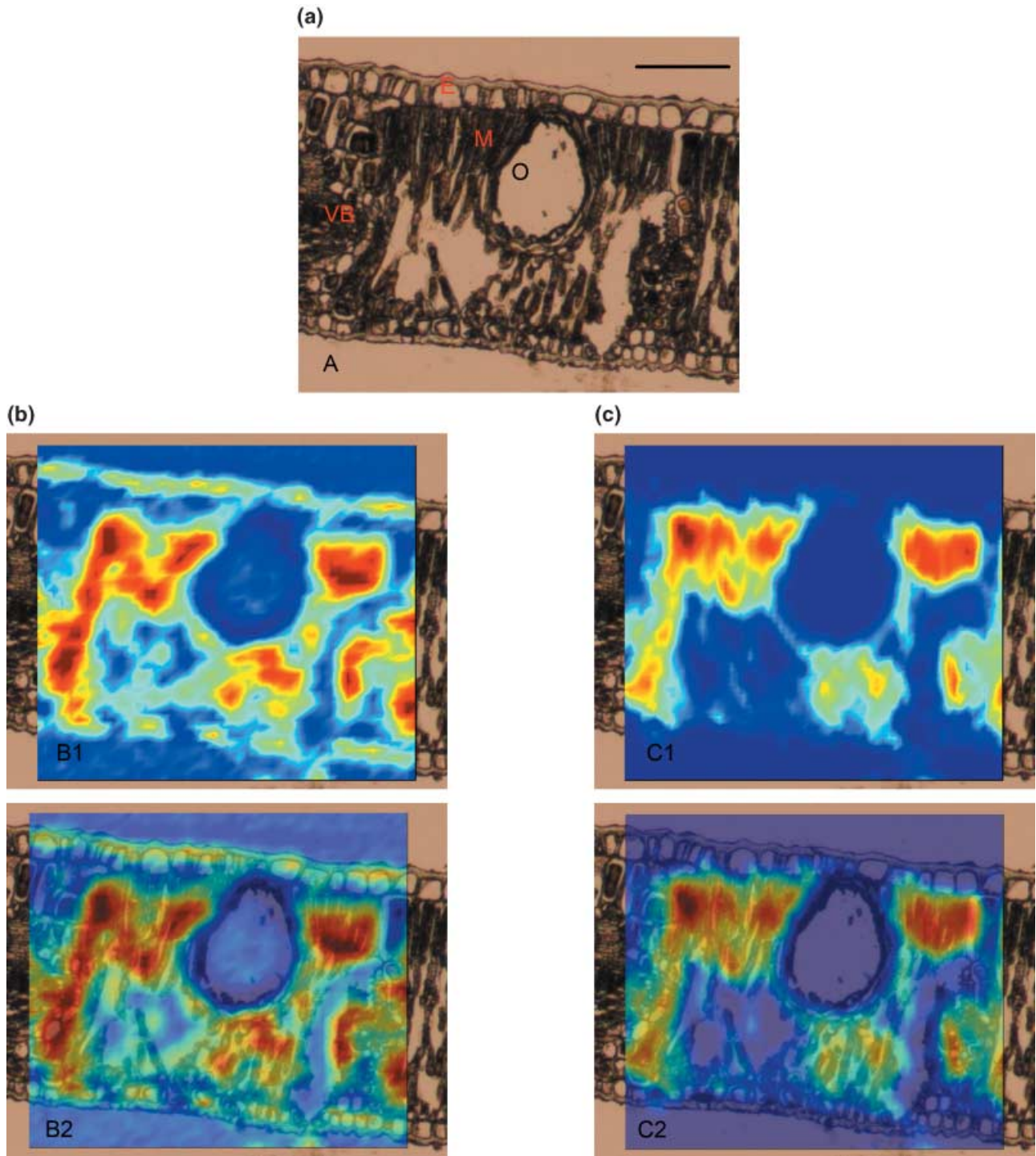


**Fig. 1** Comparisons between chemical maps of a part of a transverse section of a leaf from *Eucalyptus botryoides* achieved using Fourier transform infrared (FTIR) microspectroscopy point-to-point mapping with a synchrotron source and imaging using a focal plane array detector on an FTIR microscope with a conventional infrared source. (a) A micrograph of the transverse section. (b) The upper image shows the micrograph overlaid with a map at 50% opacity created with synchrotron infrared microspectroscopy using the integrated absorbance of a the spectral region between 1700 and 1580  $\text{cm}^{-1}$  (amide I band), attributed to protein. The lower image shows the same map as the upper image at full opacity. (c) The upper image shows the micrograph overlaid with a map at 50% opacity created with a focal plane array FTIR imaging using the integrated absorbance of the same spectral region as in the upper image in (b). The upper image in (c) shows the same map as the lower image in (c) at full opacity. A rainbow scheme has been used to denote absorbance, with the warmest colours (red end of the spectrum) indicating the highest absorbance. Bar, 100  $\mu\text{m}$ . E, epidermis; M, mesophyll; VB, vascular bundle; O, oil gland.

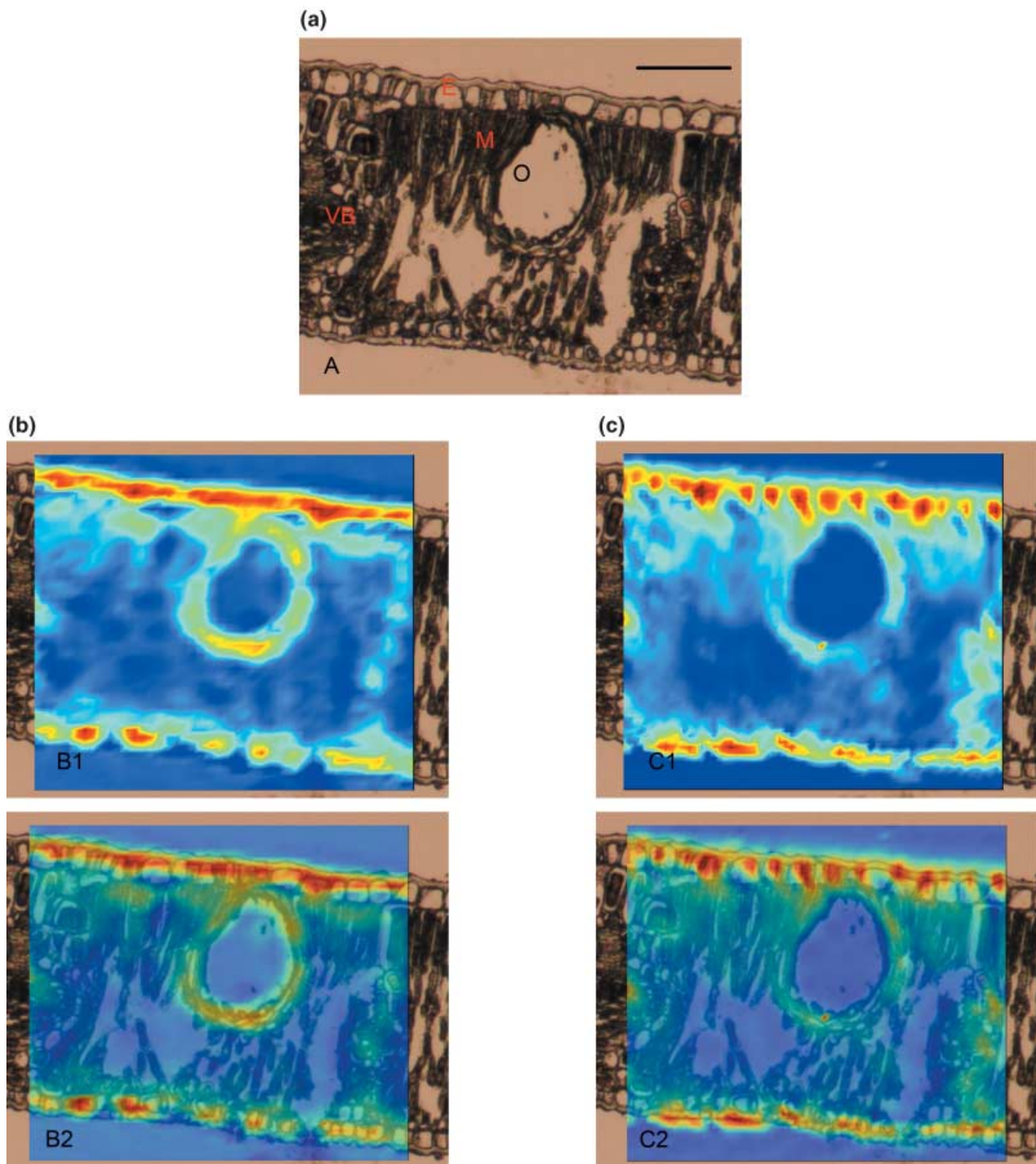


**Fig. 2** The same comparison as shown in Fig. 1 except that the spectral region between 1770 and 1700  $\text{cm}^{-1}$  (ester carbonyl), attributed mainly to lipid or lignin absorbance, was used to create the chemical maps.

(particularly the ring vibrations around 1515 and 1595  $\text{cm}^{-1}$ ) and those arising mainly from cell wall pectins (stretching vibrations from carboxylate groups at 1420  $\text{cm}^{-1}$ ). Carbonyl stretching in lignins also contributes to the band at 1730  $\text{cm}^{-1}$ , in addition to absorbance from lipids.

#### Spectral difference between tissue types

Each of the tissue types found in the leaf had a distinct spectral profile, which is shown in Fig. 3. Differences in the intensity of bands in the different cell types appeared to correspond

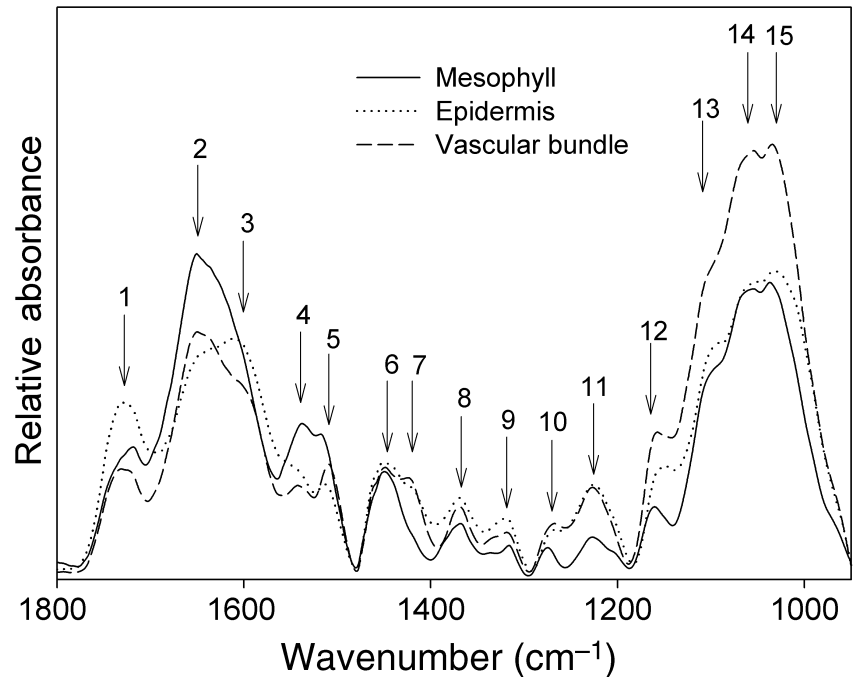


**Fig. 3** Comparison between Fourier transform infrared (FTIR) spectra acquired from spatial regions containing epidermal, mesophyll or vascular bundle (phloem and xylem) cells from a transverse section of a *Eucalyptus botryoides* leaf. Each spectrum represents the mean of approx. 40 spectra acquired using the focal plane array FTIR microscope. Fifteen of the major absorbance bands observed in the spectra are identified (see Table 1).

with the cellular chemistry reported previously for these tissue types. For instance, the mesophyll cell average spectrum had the most intense amide I absorbance compared with all the other tissue types. The amide I maximum occurred at  $1650\text{ cm}^{-1}$  in the mesophyll cell spectrum, indicating that proteins from these cells are predominantly  $\alpha$  helix in structure (Byler & Susi, 1986). This is consistent with mesophyll cells being photosynthetic cells, and hence containing a large quantity of the enzyme responsible for fixing  $\text{CO}_2$  in the chloroplasts, ribulose bis-phosphate carboxylase/oxygenase, which is known to have a predominant  $\alpha$  helical structure (Laskowski *et al.*, 1997; Heraud *et al.*, 2005). By contrast, the epidermal cell spectra had a less intense amide I absorbance, with the maximum at  $1630\text{ cm}^{-1}$ , which may indicate that there is a predominance of  $\beta$  pleated structure in the epidermal cell proteins (Byler & Susi, 1986). Of course, whether these differences in secondary structure of proteins are preserved after the chemical processing used to process the leaf tissue for FTIR spectroscopy remains subject to debate.

The spectra from the region of the vascular bundle showed prominent bands from lignin, particularly the bands at  $1515$  and  $1595\text{ cm}^{-1}$ . This is consistent with the presence of xylem in the vascular bundles. The C-O stretching region ( $1200$ – $900\text{ cm}^{-1}$ ) was also very intense in the conductive cell spectra, indicating a substantial absorbance from carbohydrate from the conductive bundle region. It is difficult to assign bands precisely in the C-O stretching region (Bonetta *et al.*, 2002), as combination bands often result from multiple deformation modes in polysaccharide molecules. Based on the spectra of crystalline cellulose, the band at  $1160\text{ cm}^{-1}$  can be assigned

to asymmetric C-O-C bridge stretch; and the bands at  $1060$  and  $1035\text{ cm}^{-1}$  can be assigned to the C-O-C stretch from pyranose rings (Cael *et al.*, 1975). Similar bands also arise from soluble carbohydrates such as various plant starches, so it is impossible to ascribe all bands in this spectral region to cellulose. Nevertheless, the strong absorbance of carbohydrate relative to protein in vascular bundle spectra is consistent with the thick cell walls and lack of cytoplasmic content in xylem cells that are found in the conductive bundles.

The carbonyl stretching band at  $1730\text{ cm}^{-1}$  results from both lipid and lignin. This band was most intense in the spectra from the epidermis and vascular bundle, and was weaker in the mesophyll spectra. The intense absorbance in the conductive bundle spectra corresponds to the presence of lignin in the xylem cells. As the epidermis is not lignified, the strong ester carbonyl absorbance from this cell type indicates a higher lipid component from epidermal compared with mesophyll cells. This must result from endogenous lipids in the epidermis itself, as paraffin does not have ester groups and any residue left after the tissues are cleared with xylene will not contribute to absorbance in this spectral region. Residual paraffin may, however, contribute to the bands at  $1450$  and  $1370\text{ cm}^{-1}$  as a result of  $\text{CH}_3$  and  $\text{CH}_2$  bending. Hence interpretation of these bands, as well as the C-H stretching bands between  $3000$  and  $2800\text{ cm}^{-1}$  (data not shown), should be carefully considered when the histological methods described here are employed to prepare tissue samples. The presence of endogenous lipids in the sections from the *E. botryoides* leaves following the alcohol dehydration and xylene washes used to prepare the samples in this study is supported by other work

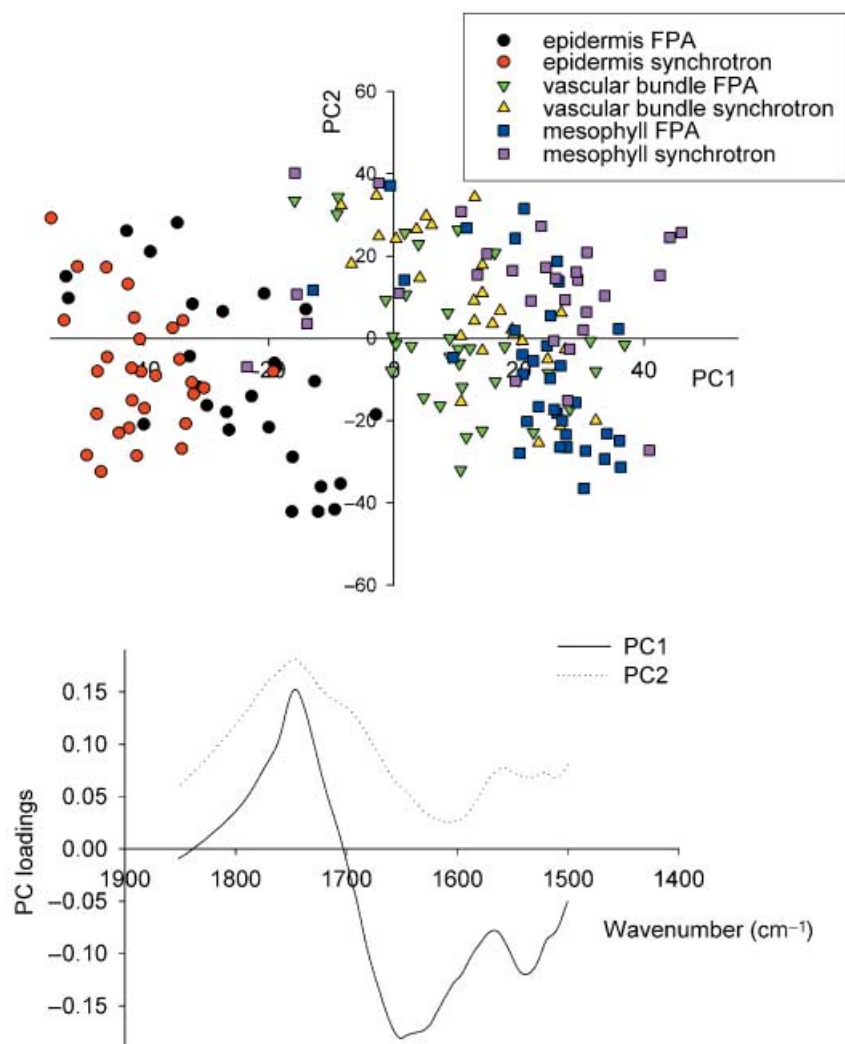


**Fig. 4** Scores and loadings plots from principal component analysis of groups of 25 independent spectra acquired from focal plane array (FPA) images and synchrotron maps of a *Eucalyptus botryoides* leaf section within spatial regions containing epidermal, mesophyll and vascular bundle tissue.

which has shown that some lipid remains in *Eucalyptus polybractea* R. T. Baker leaf sections even after weeks of exposure to solvents (King, 2006).

#### Comparison between synchrotron mapping and FPA imaging

Figures 1 and 2 show comparisons of FPA images with synchrotron maps based on amide I or ester carbonyl absorbance. The images and maps are remarkably similar to one another. This supports the view that the spectral data acquired using the two techniques are very similar both in spectral absorbance and in spatial location. For example, in Fig. 1 the highest amide I absorbance occurred in the mesophyll tissue. This is consistent with observations of average spectra discussed in the previous section. The highest areas of absorbance in this region coincided with the positions of cells, and the absorbance pattern was similar in the two measuring techniques in all samples. The positions of individual mesophyll cells appear to

be defined in both the images and the maps, which is not surprising given that these cells are *c.* 20  $\mu\text{m}$  in diameter, which is larger than the spatial resolution of both techniques.

The images in Fig. 2, based on ester carbonyl absorbance, show a completely different pattern to those based on protein. This supports the view that the mapping and imaging obtained are based on chemical difference at different locations in the samples and not changes in total spectral absorbance. Ester carbonyl absorbance, for example, appears to be concentrated in the epidermal cells, both on the leaf boundaries and in cells surrounding the oil gland, and in the vascular bundles. The absorbance in the vascular bundles is probably attributable to lignin, as maps contrasted using the lignin band at 1515  $\text{cm}^{-1}$  showed intense absorbance only at the positions of the vascular bundles (data not shown). The absorbance in the epidermal region must be from lipid, as these tissues are not lignified. This is corroborated by a lack of absorbance from the 1515  $\text{cm}^{-1}$  band in the epidermal regions (data not shown). The strong lipid absorbance in the epidermal cells

may be attributable to oils and waxes that are produced in these cells and subsequently excreted into the oil gland or onto the leaf surface (Wirthensohn *et al.*, 2000).

### Principal component analysis

Spectral data are multivariate by nature and, as such, average spectra may hide trends occurring across bands in a group of spectra. PCA has proved to be a useful method for the analysis of spectral data acquired from plant tissue (Chen *et al.*, 1998). Scores plots allow one to visualize any clustering in a dataset. Preliminary analysis of the data involved PCA of groups of 25 spectra extracted from regions of both synchrotron maps and FPA images associated with epidermis, mesophyll and vascular bundle tissue regions using the entire spectral region from 2000 to 950  $\text{cm}^{-1}$ . This showed general clustering of the three tissue types mainly along PC1 with loadings plots indicating that the majority of the variation along PC1 was explained by spectral difference in the 1800–1500  $\text{cm}^{-1}$  range (data not shown). Accordingly, PCA was performed using the 1800–1500  $\text{cm}^{-1}$  range (Fig. 4) which showed the three tissue types clustering into distinct groups, with the separation occurring along PC1. The most delineated cluster was the spectra from epidermal region, with all spectra having negative PC1 scores. Spectra from mesophyll and vascular bundle tissue regions overlapped to some degree along PC1, with mesophyll spectra more variable than spectra from the vascular bundle region; nevertheless, mesophyll spectra generally had more positive PC1 scores compared with vascular bundle spectra. The loadings for the first PC showed an opposite correlation between bands in the 1700–1500  $\text{cm}^{-1}$  and 1800–1700  $\text{cm}^{-1}$  spectral ranges. This supports the view, discussed in the previous section, based on observation of the chemical maps and the average spectra, that the three tissue types vary in amide (1650 and 1540  $\text{cm}^{-1}$ ) and ester carbonyl absorbance (1730  $\text{cm}^{-1}$ ), as well as absorbances attributed to lignin (1515  $\text{cm}^{-1}$  and 1595  $\text{cm}^{-1}$ ). In general, spectra acquired using the FPA and synchrotron techniques coincided on the PC1 vs PC2 scores plot, supporting the view that the spectral data acquired using the two techniques were very similar, and spectral differences in leaf tissue can be revealed independently of which technique is employed.

### Conclusions

This study shows that FPA imaging can achieve very similar results to synchrotron FTIR microspectroscopic mapping of leaves. A comparison of the maps and images produced suggests that both techniques are capable of resolving chemical differences in leaf tissue at the single cell level. Multivariate data analysis revealed chemical differences among the various tissue types in the leaf, regardless of the measurement techniques employed.

The main advantage of the laboratory-based FPA technique is that the expense and limited access to synchrotrons can be

avoided, and the FPA measurements are much more rapid compared with the synchrotron-based mapping; however, this is achieved at a slightly lower spatial resolution and a reduced signal-to-noise ratio compared with the synchrotron-based method, although using more spectral scans with the FPA measurement could nullify the signal-to-noise ratio disparity. The histological technique developed here is especially suited to sclerophyllous leaves, but should be equally applicable to other plant tissues, for the reliable, inexpensive and consistent preparation of samples for FPA or synchrotron analysis.

Importantly, this study demonstrates that FPA imaging data can be used to differentiate the major tissue types in the leaf, with each shown to have a unique 'biochemical fingerprint' or spectral phenotype, which can be modelled using multivariate data analysis methods. This finding points the way towards a number of exciting experimental possibilities. For example, phenotypic characterization of tissues using FPA spectroscopic imaging should enable the tracking of chemical changes in plant tissues, both spatially and temporally, during development and senescence. Another exciting possibility is the monitoring of the chemical nature of disease processes in plant tissues caused by pathogens, toxins or pollutants. Recently, there has been an explosion of applications in human medicine using infrared spectroscopic imaging with multichannel detectors yielding many powerful insights (Bhargava & Levin, 2005); the application of these methods in the plant sciences holds similar promise.

### Acknowledgements

The authors would like to acknowledge the expert assistance of Mr Ian Boundy from the Monash University Histology Laboratory for his advice on the histological methods, Dr Michael Martin from the Advanced Light Source, Berkeley, CA, for his assistance with the infrared microspectroscopic mapping, and Mr Finlay Shanks from the Monash University Centre for Biospectroscopy and Mr Mustafa Kansiz from Varian Analytical Instruments for their assistance and advice on the focal plane array imaging.

### References

- Bamberg KR, Wood BR, Quinn MA, McNaughton D. 2004. Fourier transform infrared imaging and unsupervised hierarchical clustering applied to cervical biopsies. *Australian Journal of Chemistry* 57: 1139–1143.
- Bandekar J. 1992. Amide modes and protein conformation. *Biochimica Biophysica Acta* 1120: 123–143.
- Barron C, Parker ML, Mill ENC, Rauou X, Wilson RH. 2005. FTIR imaging of wheat endosperm cell walls in situ reveals a compositional and architectural heterogeneity related to grain hardness. *Planta* 220: 667–677.
- Bhargava R, Levin IW. 2005. *Spectrochemical analysis using infrared multichannel detectors*. Oxford, UK: Blackwood.
- Bociek SM, Welti D. 1975. The quantitative analysis of uronic acid polymers by infrared spectroscopy. *Carbohydrate Research* 42: 217–226.

- Bonetta DT, Facette M, Raab TK, Somerville CR. 2002. Genetic dissection of cell wall biosynthesis. *Biochemical Society Transactions* 30: 298–301.
- Byler DM, Susi H. 1986. Examination of the secondary structure of proteins by deconvolved FTIR spectra. *Biopolymers* 25: 469–487.
- Cael JJ, Gardner KH, Koenig JL, Blackwell J. 1975. Infrared and Raman spectroscopy of carbohydrates. V. Normal coordinate analysis of cellulose I. *Journal of Chemical Physics* 62: 1145–1153.
- Chen L, Carpita NC, Reiter W-D, Wilson RH, Jeffries C, McCann MC. 1998. A rapid method to screen for cell wall mutants using discriminant analysis of Fourier infrared transform spectra. *The Plant Journal* 16: 385–392.
- Colthup NB, Daly LH, Wiberley SE. 1964. *Introduction to infrared and Raman spectroscopy*. New York, NY, USA: Academic Press.
- Dokken KM, Davis LC. 2005. Use of infrared microspectroscopy in plant growth and development. *Applied Spectroscopy Reviews* 40: 301–326.
- Faix O. 1992. Fourier transform infrared spectroscopy. In: Lin SY, Dence CW, eds. *Methods in lignin chemistry*. New York, NY, USA: Springer-Verlag, 83–106.
- Giordano M, Kansiz M, Heraud P, Beardall J, Wood BR, McNaughton D. 2001. Fourier transform infrared spectroscopy as a novel tool to investigate changes in intracellular macromolecular pools in the marine microalga *Chaetoceros muellerii* (Bacillariophyceae). *Journal of Phycology* 37: 271–279.
- Heraud P, Wood BR, Tobin MJ, Beardall J, McNaughton D. 2005. Mapping of nutrient-induced biochemical changes in living algal cells using synchrotron infrared microspectroscopy. *FEMS Microbiology Letters* 249: 219–225.
- Himmelsbach DS, Khalili S, Aitkin DE. 1998. FTIR microspectroscopic imaging of flax (*Linum usitatissimum* L.) stems. *Cellular and Molecular Biology* 44: 99–108.
- Kačuráková M, Capek P, Sasinková V, Wellner N, Ebringerová A. 2000. FTIR study of plant cell wall compounds: pectic polysaccharides and hemicelluloses. *Carbohydrate Polymers* 43: 195–203.
- Kačuráková M, Wilson RH. 2001. Developments in mid infrared FTIR spectroscopy of selected carbohydrates. *Carbohydrate Polymers* 44: 291–303.
- Kansiz M, Heraud P, Wood BR, Beardall J, Burden F, McNaughton D. 1999. Fourier transform infrared microspectroscopy and chemometrics as a tool for the discrimination of cyanobacterial strains. *Phytochemistry* 52: 407–417.
- King DJ. 2006. Regulation of oil accumulation in *Eucalyptus polybractea*. PhD Thesis, The University of Melbourne, Australia.
- Laskowski RA, Hutchinson EG, Michie AD, Wallace AC, Jones ML, Thornton JM. 1997. PDBsum: a Web-based database of summaries and analyses of all PDB structures. *Trends in Biochemical Sciences* 22: 488–490.
- Levenson E, Lerch P, Martin MC. 2006. Infrared imaging: Synchrotrons vs. arrays, resolution vs. speed. *Infrared Physics & Technology* 49: 45–52.
- Martin MC, McKinney WR. 1998. The first infrared beamlines at the advanced light source: microspectroscopy and fast timing. *Proceedings of the Materials Research Society* 524: 11–16.
- Mills ENC, Parker NL, Wellner N, Toole G, Feeney K, Shewry PR. 2005. Chemical imaging: the distribution of ions and molecules in developing wheat grains. *Journal of Cereal Science* 43: 193–201.
- Nelson WH. 1991. *Modern techniques for rapid microbiological analysis*. New York, NY, USA: VCH Publishers.
- Thennadil SN, Martens H, Kohler A. 2006. Physics based multiplicative scatter correction approaches for improving the performance of calibration models. *Applied Spectroscopy* 60: 315–321.
- Williams DH, Fleming I. 1996. *Spectroscopic methods in organic chemistry, 5th edn*. London, UK: McGraw-Hill International.
- Wirthensohn MG, Sedgley A, Jones GP. 2000. Epicuticular wax of juvenile Eucalyptus leaves and headspace analysis of leaf volatiles. *Journal of Essential Oil Research* 12: 401–411.
- Wong PTT, Wong RH, Caputo TA, Godwin TA, Rigas B. 1991. Infrared spectroscopy of exfoliated human cervical cells: evidence of extensive structural changes during carcinogenesis. *Proceedings of the National Academy of Sciences, USA* 88: 10988–10992.
- Wood BR, Chiriboga L, Quinn MA, McNaughton D, Diem M. 2005. Fourier transform infrared (FTIR) spectral imaging of the cervical transformation zone and dysplastic squamous epithelium. *Gynecological Oncology* 93: 59–68.
- Zeroual W, Choisy C, Doglie SM, Bobichon H, Angiboust J, Manfait M. 1994. Monitoring of bacterial growth and structural analysis as probed by FT-IR spectroscopy. *Biochimica Biophysica Acta* 1222: 171–178.